

Friction of Ultrathin Amorphous Carbon Films Synthesized by Filtered Cathodic Vacuum Arc and Radio-Frequency Sputtering

J. Matlak and K. Komvopoulos*

Department of Mechanical Engineering, University of California, Berkeley, CA 94720, USA

Abstract

The friction properties of ultrathin amorphous carbon (*a*-C) films deposited on Si(100) substrates by radio-frequency sputtering and filtered cathodic vacuum arc were investigated by surface force microscopy. Deposition parameters yielding *a*-C films with high sp^3 content were used to synthesize films of thickness between 5 and 35 nm. The coefficient of friction of both types of *a*-C films was measured with a 1- μ m-radius conical diamond tip and normal loads in the range of 20–640 μ N. The results show a strong dependence of the friction characteristics on film surface roughness, thickness, and structure. The dependence of the coefficient of friction on normal load and the dominance of adhesion and plowing friction mechanisms are interpreted in terms of the through-thickness variation of carbon atom hybridization of the *a*-C films.

*Corresponding author: K. Komvopoulos (e-mail: kyriakos@me.berkeley.edu)

Submitted to *IEEE Transactions on Magnetics* on May 30, 2014.

I. INTRODUCTION

Amorphous carbon (*a*-C) films are of particular interest because their unique properties (i.e., high hardness, low friction, high wear resistance, chemical inertness, low magnetic susceptibility, and large optical band gap) are critical to many industrial and medical applications, including magnetic storage devices, microelectromechanical systems, and biomedical/implantable components [1]–[4]. Several deposition methods have been used to synthesize carbon films, such as radio-frequency (RF) sputtering, ion-beam deposition, laser ablation, and filtered cathodic vacuum arc (FCVA). Depending on the deposition method and associated process parameters, film quality is strongly affected by the film surface roughness, uniformity, and structure (carbon atom bonding). Considering the industrial relevance of ultrathin *a*-C films, characterization of the friction properties of these films is of high importance.

A prominent application of *a*-C films is in magnetic recording devices where maintaining the integrity of the stored data is critical. In hard-disk drives, information is stored in the magnetic medium (e.g., CoCrPt or FeNi) of a hard disk by the magnetic field of a read/write transducer embedded at the trailing edge of the head. To preserve the reliability of magnetic storage devices, ultrathin *a*-C films are used as overcoats to protect the hard disk and magnetic head against mechanical wear and corrosion [5]. In addition, a lubricant monolayer adsorbed onto the carbon overcoat reduces adhesion at the head-disk interface whenever intermittent asperity-asperity contact is encountered during operation. Because of the exponential increase in data storage density with decreasing magnetic spacing, the trend is to reduce the physical spacing between the read/write transducer and the magnetic medium by thinning the carbon overcoat to a few nanometers. With such ultrathin overcoats, the storage density may be increased from several hundreds of Gbit/in² to several Tbit/in² [6]–[8]. Decreasing the carbon overcoat thickness to a few nanometers, while preserving the mechanical and tribological properties and preventing corrosion of the magnetic medium, presents a challenging task of high technological importance.

The structure of *a*-C films is characterized by the short-range order of carbon atoms in linear (sp^1), trigonal (sp^2), and tetrahedral (sp^3) configurations [9]. While sp^2 hybridization (graphite-like) has

both σ and π bonds, sp^3 hybridization (diamond-like) has only σ bonds. The stronger σ bonds control the mechanical properties, whereas the weaker π bonds affect the electrical and optical properties [10]. Hard a -C films with high sp^3 content form three-dimensional metastable amorphous networks that exhibit various levels of intermediate-range order [11]. Correlating the sp^3 content with the friction characteristics of ultrathin a -C films requires the use of surface-sensitive probe-based mechanical testing and knowledge of through-thickness film structure.

Several deposition methods can be used to synthesize ultrathin a -C films, including FCVA, pulsed laser deposition, plasma-assisted chemical vapor deposition, and RF sputtering [12]–[16]. The film structure and mechanical properties depend on the deposition method and associated process parameters, such as plasma power, substrate bias voltage (ion kinetic energy), ion fluence, and ion incidence angle. The mechanical and tribological properties of a -C films can be influenced by the film structure (sp^3/sp^2 ratio), hydrogen content, and adhesive strength to the substrate, all of which depend on the particular deposition method. In general, high sp^3 content correlates with high hardness [17]. The sp^3/sp^2 ratio tends to decrease in the following ranking of deposition method: FCVA, pulsed laser vaporization, direct ion-beam deposition, plasma-enhanced chemical vapor deposition, ion-beam sputtering, and sputtering [18].

The main objective of this study is to elucidate the dependence of the friction properties of ultrathin (5–35 nm thick) a -C films deposited by FCVA and RF sputtering on corresponding surface roughness, thickness, and structure. Key deposition parameters of each deposition process were configured such that to maximize the sp^3 content of both FCVA and sputtered a -C films. The friction behavior is interpreted in terms of adhesion and plowing mechanisms affected by the surface roughness and through-thickness structure of the deposited films.

II. EXPERIMENTAL METHODS

Substrates for both FCVA and RF sputtering deposition experiments were obtained by sectioning p-type Si(100) wafers into $10 \times 10 \text{ mm}^2$ pieces. The substrates were then cleaned by rinsing with isopropanol and acetone for 10 min each and, finally, blow drying with nitrogen gas.

A. *Filtered Cathodic Vacuum Arc*

FCVA is ideal for low-temperature deposition of continuous ultrathin smooth films on various substrates without the need of an adhesion underlayer. Technical improvements (especially to plasma stabilization and filtering) have offset early problems with plasma instabilities, difficulties with particle filtering, and poor film adhesion onto electrically insulating substances [19]. The FCVA system used in the present study utilizes a vacuum arc plasma source to deposit a film onto a substrate. The process relies on the ignition of a vacuum electric arc between an anode and a cathode consisting of a high purity material (99.99% pure graphite in this study). During arc discharging, electrons flowing from the cathode generate both pressure and electrical potential gradients, refocusing the arc on fluctuating small spots at the cathode surface. The resulting pressure gradients close to the cathode surface result in the ejection of cathode material in the form of plasma, which is then guided by upstream, auxiliary, and downstream coils toward a rotating substrate holder to ensure uniform film deposition. Four orthogonally mounted raster coils positioned outside the downstream coil raster the plasma beam. To stabilize the arc discharges, a “cusp” configuration magnetic field is generated by superposing the magnetic fields generated by the cathode and upstream anode coils. The out-of-plane S-shaped configuration of the magnetic filter prevents macroparticles and/or droplets that may be ejected from the cathode from depositing onto the film surface. Water cooling removes any excess heat at the substrate holder. The film quality strongly correlates with the C^+ ion energy and substrate bias voltage. The increase of the ion energy causes intense collisions between C^+ ions and substrate atoms, promoting sp^3 hybridization. Too high of an ion energy, however, can also result in thermal relaxation, which is conducive to $sp^3 \rightarrow sp^2$ rehybridization [22]. Therefore, optimal C^+ ion energy of ~ 120 eV is used to balance these opposing processes and to maximize the sp^3 fraction and hardness of the FCVA films [21].

After mounting the samples onto the substrate holder, the chamber was pumped down to a base pressure of less than 5×10^{-7} Torr with a cryopump. Before initiating film deposition, the native SiO_2 layer and any adsorbents were removed by bombarding the silicon substrate with 500-eV Ar^+ ions generated by a 64-mm Kaufman ion source. This cleaning step was performed for 2 min at a pressure of 2

$\times 10^{-4}$ Torr and an Ar^+ ion incidence angle of 60° relative to the substrate normal. In all film depositions, the base pressure was less than 5×10^{-7} Torr and a pulsed bias voltage of -100 V and 25 kHz frequency was applied to the substrate. The deposition time were varied to obtain films of thickness in the range of 6–35 nm. More details about the FCVA system used in this study can be found elsewhere [19]. The deposition parameters and thickness of the FCVA *a*-C films examined in this study are given in Table I.

B. Radio-Frequency Sputtering

RF sputtering enables fast deposition of carbon films at working pressures less than those of FCVA, resulting in less gas molecule collisions and enhanced line-of-sight deposition. In addition, reversing the polarity prevents charging effects and reduces arcing. Unlike FCVA, RF sputtering does not produce continuous films with thickness less than 5 nm, because initial film growth is characterized by the formation of small islands, which eventually coalesce to form a continuous film when an effective film thickness of ~ 5 nm is reached. Because the sp^3 content of sputtered films is usually less than that of FCVA films, the hardness of sputtered *a*-C films is normally less than that of FCVA *a*-C films.

In RF sputtering, a glow discharge is produced by an RF power source in a vacuum chamber under pressure-control flow of an inert gas (usually Ar). Sufficient ion momentum transfer to the graphite target surface causes the ejection of carbon atoms or clusters of carbon atoms, which travel through the plasma and deposit onto the substrate surface to form a carbon film. Because individual atoms are chemically active, inert gas prevents the formation of undesirable compounds. The build-up of a positive electric charge on the target surface due to impinging plasma ions is avoided by applying an RF voltage to the target assembly, which reverses the polarity by attracting enough electrons from the discharge.

Film deposition by RF sputtering comprised first pumping down the chamber to a base pressure of less than 5×10^{-6} Torr with a cryopump, introducing Ar gas at a flow rate of 20 sccm, and then raising the chamber pressure to 3 mTorr by adjusting the throttle valve. Before each film deposition, the graphite target was sputter-cleaned for 10 min and the Si(100) substrate for 3 min to remove the native SiO_2 layer, both processes performed at 250 W power and 3 mTorr working pressure in pure Ar plasma. The self-

biased target voltage ranged from -750 to -850 V during cleaning of the substrate surface, and between -980 and -1000 V during target cleaning. The film quality strongly correlates to the RF power and substrate bias voltage. An optimal forward RF power of 750 W and a substrate bias voltage of -200 V maximize the film hardness and elastic modulus, while minimizing friction and surface roughness [22]. Under these sputtering conditions, bombarding Ar^+ ions effectively eliminate weakly bonded carbon atoms without damaging the film structure. During film deposition, therefore, the substrate bias voltage and forward RF power were set to -200 V and 750 W, respectively. The deposition time was varied to produce films of thickness in the range of 5 – 35 nm. The deposition parameters and thickness of the sputtered *a*-C films examined in this study are given in Table II.

C. Surface Topography Characterization

The film surface topography was studied with an atomic force microscope (AFM, Dimension 3100, Veeco Metrology Group, Digital Instruments) operated in tapping mode at a frequency of ~ 300 kHz. Highly-doped, n-type, single-crystal Si tips of conical shape (Aspire CT-300, Nanoscience Instruments) with a nominal radius of curvature equal to ~ 8 nm were used to scan $2 \times 2 \mu\text{m}^2$ surface areas at a speed of $2 \mu\text{m/s}$. For statistical analysis, surface imaging and root-mean-square (rms) roughness calculations were performed for five different surface areas of each film.

D. Friction Testing

The friction characteristics of the deposited *a*-C films were studied with a scanning force microscope (SFM) consisting of an AFM (Nanoscope II, Digital Instruments) retrofitted with a capacitive force transducer (Triboscope, Hysitron) consisting of two three-plate capacitors, which enable highly sensitive displacement and force measurements in the normal and horizontal directions relative to the sample surface. AFM and transducer controllers are used for both operation and data acquisition. A control unit provides force readout and offset, gain control, and filtering of microscope *z*-feedback.

All friction tests were performed with a conical diamond tip of radius of curvature equal to $1 \mu\text{m}$. To relate the tip contact area to the indentation (contact) depth, a polynomial tip-shape function was

determined from several indentations performed on a standard smooth sample of fused quartz of hardness and reduced elastic modulus equal to 10 and 69.6 GPa, respectively. The tip calibration procedure was frequently repeated to account for changes in the tip shape affecting the tip-shape function.

During friction testing, the load was increased to a peak value in the range of 20–640 μN at a rate of 20 $\mu\text{N/s}$, kept at that value for 10 s, and finally decreased to zero at a constant unloading rate of 20 $\mu\text{N/s}$. The sliding speed and lateral displacement were set to 0.33 $\mu\text{m/s}$ and 10 μm , respectively, and the distance between sliding tracks was larger than 1 μm . A total of 300 data sets of normal and lateral force and displacement measurements were collected from each friction test. The friction force and normal displacement were calculated as averages of ten measurements. The coefficient of friction was determined as the ratio of the measured friction force to the applied load. Steady-state coefficients of friction were calculated as averages of coefficient of friction values corresponding to the final 7 μm of the sliding track. For statistical analysis and to ensure reproducibility, all friction tests were repeated at least five times on different surface areas of each film.

III. RESULTS AND DISCUSSION

Figs. 1 and 2 show representative surface topography images of FCVA and sputtered films, respectively. A qualitative comparison of the AFM images indicates roughening of the surface topography with increasing film thickness for both films. This trend is more apparent for sputtered films. Fig. 3 shows the average rms roughness of FCVA and sputtered films as a function of film thickness. Both films show significant surface roughening above a critical film thickness, characteristic of the deposition process. However, FCVA films show significantly lower surface roughness than sputtered films regardless of film thickness. The rms roughness of the Si(100) substrate is equal to ~ 0.20 nm, which is much higher than the roughness of the FCVA films, but close to the roughness of sputtered films. The average roughness of sputtered films decreases from 0.194 nm to 0.188 nm with the increase in film thickness from 5 to 20 nm and sharply increases to 0.214 nm when the film thickness is increased to 35 nm. The average roughness

of FCVA films first decreases from 0.131 nm to 0.123 nm with film thickness increasing from 6 to 10 nm, then sharply increasing to 0.173 nm with film thickness increasing in the range of 10–35 nm.

Differences in the film surface topography may be attributed to deposition process intricacies. Film-forming precursors in sputtering are atoms and/or clusters of atoms as opposed to energetic C^+ ions in FCVA. Thus, in the early stage of film deposition, sputtered films demonstrate island-like growth, while FCVA film growth is an atomic-level process involving simultaneous carbon implantation and re-sputtering of the growing film, depending on C^+ ion energy. Hence, the lower roughness of FCVA films is attributed to the much finer scale of film deposition than sputtering and the re-sputtering effect of bombarding energetic C^+ ions.

Fig. 4 shows the coefficient of friction of FCVA and sputtered *a*-C films as a function of sliding distance, film thickness, and applied load. A steady-state coefficient of friction is reached after a short sliding distance of ~ 2 μm . In general, the coefficient of friction increases with applied load. This is better illustrated in Fig. 5 showing the variation of the steady-state coefficient with load. With the exception of the thinner (5–7 nm) films, all other films show a minimum coefficient of friction at a critical load regardless of deposition method, a trend that is more pronounced for thicker films. Comparison of the results shown in Figs. 4 and 5 reveals several notable trends. First, the steady-state coefficient of friction of sputtered films is less than that of FCVA films regardless of load and film thicknesses. Second, the coefficient of friction first decreases and then increases with increasing load except for very thin (5–7 nm) films. Such phenomena may be explained by considering the multilayered structure of *a*-C films, particularly the composition and carbon bonding in each layer present in the through-thickness film structure, and the interaction between the diamond tip and the films in terms of the contact depth and associated dominant friction mechanisms.

The through-thickness distribution of hybridized carbon atoms greatly influences the friction behavior of *a*-C films because different types of hybridization yield different mechanical properties. Specifically, the softer sp^2 hybridization imparts graphite-like behavior, while the stronger sp^3

hybridization yields diamond-like behavior. An increase in sp^2 content may thus produce lower friction as a result of the predominantly graphitic structure of the film. This appears to be the case when comparing the friction characteristics of FCVA and sputtered films (Figs. 4 and 5), where sputtered films possessing higher sp^2 concentrations consistently exhibit lower coefficient of friction than FCVA films. Consequently, despite the higher roughness of sputtered films, the main differences in the friction properties of FCVA and sputtered films may be attributed to differences in the shear resistance (plastic flow) controlled by through-thickness film structure. However, a direct comparison of coefficients of friction under different loads cannot be made without considering the dominant friction mechanisms of each film.

Depending on contact depth, different concentrations of sp^2 and sp^3 bonding were encountered by the sliding diamond tip, affecting the film friction behavior. FCVA ultrathin *a*-C films demonstrate a four-layer structure comprising an interface (intermixing) layer consisting of C, Si, and, possibly, SiC, buffer layer with continuously increasing sp^3 content, bulk film showing high and constant sp^3 concentration, and ultrathin surface layer rich in sp^2 hybridization [20]. The interface layer has relatively low sp^3 content due to low carbon concentration resulting from carbon intermixing with Si and possible formation of SiC. The sp^3 content of the buffer layer (a thin layer of pure carbon forming after the interface layer) significantly increases toward the interface with the bulk film. When the film thickness exceeds the penetration range of the impinging C^+ ions, only carbon bonding exists and the development of a compressive stress because of the subplantation effect promotes sp^3 hybridization, leading to the formation of the bulk film with high and constant sp^3 concentration. The surface layer exhibits higher sp^2 content due to less C^+ ion bombardment. An analogous trend in carbon atom bonding distribution has been reported for RF sputtered films, with higher sp^3 contents determined for the bulk layer than the interface layer [23], though the overall sp^3 concentration is generally less than that of FCVA films. In light-load sliding, therefore, the diamond tip mostly interacted with the thin sp^2 -rich surface layer of the films, resulting in low friction because the graphite-like surface layer acted as a solid lubricant film. However, high-load sliding resulted

in plowing through the sp^3 -rich bulk film, which exhibits much higher shear resistance than the surface layer. In addition, because the silicon substrate is more compliant than the a -C films, the contact area also increased with the load, resulting in greater contribution of adhesion to the total friction force. Thus, the increase of the coefficient of friction with load above a critical load value (Fig. 5) is attributed to the enhancement of both plowing and adhesion friction mechanisms.

IV. CONCLUSION

An investigation of the friction characteristics of ultrathin a -C films deposited on Si(100) substrates by FCVA and RF sputtering revealed a strong dependence on the film surface roughness, thickness, and through-thickness structure (atomic bonding). The sputtered films demonstrated notably lower friction than FCVA films of similar thickness because of the lower surface shear resistance to plastic flow due to the higher sp^2 content of these films. Differences in the sliding friction behaviors of FCVA and sputtered films are attributed to variations in the through-thickness film structure, which is intrinsic of the deposition process, and dominance of different friction mechanisms (adhesion and plowing) at different contact depths (loads).

ACKNOWLEDGMENT

This research was funded by the Computer Mechanics Laboratory, University of California, Berkeley.

REFERENCES

- [1] A. H. Lettington, "Applications of Diamond-Like Carbon Thin Films," *Phil. Trans. R. Soc. London, Ser. A*, vol. 342, pp. 287–290, 1993.
- [2] J. Robertson, "Ultrathin Carbon Coatings for Magnetic Storage Technology," *Thin Solid Films*, vol. 383, pp 81–88, 2001.
- [3] T. S. Santra, T. K. Bhattacharyya, P. Patel, F. G. Tseng, and T. K. Barik, "Diamond, Diamond-Like Carbon (DLC) and Diamond-Like Nanocomposite (DLN) Thin Films for MEMS Applications," *Microelectromechanical Systems and Devices*, N. Islam (editor), InTech, pp. 459–480, 2006

- [4] A. Grill, "Diamond-Like Carbon Coatings as Biocompatible Materials – An Overview," *Diamond Relat. Mater.*, vol. 12, pp. 166–170, 2003.
- [5] N. Yasui, H. Inaba, K. Furusawa, M. Saito, and N. Ohtake, "Characterization of Head Overcoat for 1 Tb/in² Magnetic Recording," *IEEE Trans. Magn.*, vol. 45, pp. 805–809, 2009.
- [6] R. Wood, "Future Hard Disk Drive Systems," *J. Magn. Magn. Mater.*, vol. 321, pp. 555–561, 2009.
- [7] Z. Z. Bandić and R. H. Victora, "Advances in Magnetic Data Storage Technologies," *Proc. IEEE*, vol. 96, pp. 1749–1753, 2008.
- [8] Z.-M. Yuan, B. Liu, T. Zhou, C. K. Goh, C. L. Ong, C. M. Cheong, and L. Wang, "Perspectives of Magnetic Recording System at 10 Tb/in²," *IEEE Trans. Magn.*, vol. 45, pp. 5038–5043, 2009.
- [9] J. Robertson, "Diamond-Like Amorphous Carbon," *Mater. Sci. Eng. R*, vol. 37, pp. 129–281, 2002.
- [10] J. Robertson, "Amorphous Carbon," *Adv. Phys.*, vol. 35, pp. 317–374, 1986.
- [11] D. R. McKenzie, "Tetrahedral Bonding in Amorphous Carbon," *Rep. Prog. Phys.*, vol. 59, pp. 1611–1664, 1996.
- [12] O. R. Monteiro, "Thin Film Synthesis by Energetic Condensation," *Annu. Rev. Mater. Res.*, vol. 31, pp. 111–137, 2001.
- [13] I. G. Brown, "Cathodic Arc Deposition of Films," *Annu. Rev. Mater. Sci.*, vol. 28, pp. 243–269, 1998.
- [14] A. A. Voevodin and M. S. Donley, "Preparation of Amorphous Diamond-Like Carbon by Pulsed Laser Deposition: A Critical Review," *Surf. Coat. Technol.*, vol. 82, pp. 199–213, 1996.
- [15] M. K. Fung, K. H. Lai, C. Y. Chan, I. Bello, C. S. Lee, S. T. Lee, D. S. Mao, and X. Wang, "Mechanical Properties and Corrosion Studies of Amorphous Carbon on Magnetic Disks Prepared by ECR Plasma Technique," *Thin Solid Films*, vol. 368, pp. 198–202, 2000.
- [16] W. Lu and K. Komvopoulos, "Nanotribological and Nanomechanical Properties of Ultrathin Amorphous Carbon Films Synthesized by Radio Frequency Sputtering," *ASME J. Tribol.*, vol. 123, pp. 641–650, 2001.

- [17] J. J. Cuomo, D. L. Pappas, J. Bruley, J. P. Doyle, and K. L. Saenger, "Vapor Deposition Processes for Amorphous Carbon Films with sp^3 Fractions Approaching Diamond," *J. Appl. Phys.*, vol. 70, pp. 1706–1711, 1991.
- [18] B. K. Gupta and B. Bhushan, "Mechanical and Tribological Properties of Hard Carbon Coatings for Magnetic Recording Heads," *Wear*, vol. 190, pp. 110–122, 1995.
- [19] H.-S. Zhang and K. Komvopoulos, "Direct-Current Cathodic Vacuum Arc System with Magnetic-Field Mechanism for Plasma Stabilization," *Rev. Sci. Instrum.*, vol. 79, pp. 073905(1)–073905(7), 2008.
- [20] N. Wang and K. Komvopoulos, "The Multilayered Structure of Ultrathin Amorphous Carbon Films Synthesized by Filtered Cathodic Vacuum Arc Deposition," *J. Mater. Res.*, vol. 28, pp. 2124–2131, 2013.
- [21] H.-S. Zhang and K. Komvopoulos, "Synthesis of Ultrathin Carbon Films by Direct Current Filtered Cathodic Vacuum Arc," *J. Appl. Phys.*, vol. 105, pp. 083305(1)–083305(7), 2009.
- [22] J. Xie and K. Komvopoulos, "Effect of Substrate Bias Voltage on Hybridization and Tribomechanical Properties of Ultrathin Amorphous Carbon Films Deposited by Radio-Frequency Sputtering," *J. Phys. D: Appl. Phys.*, 2014 (submitted).
- [23] D. Wan and K. Komvopoulos, "Transmission Electron Microscopy and Electron Energy Loss Spectroscopy Analysis of Ultrathin Amorphous Carbon Films," *J. Mater. Res.*, vol. 19, pp. 2131–2136, 2004.

Table I. Deposition parameters and thickness of FCVA *a*-C films.*

Film thickness (nm)	Incidence angle (deg.)	Substrate bias voltage (V)	Deposition time (s)
6–7	20	–100	30
10	10	–100	12
20	45	–100	30
35	90	–100	30

*C⁺ ion energy \approx 120 eVTable II. Deposition parameters and thickness of RF sputtered *a*-C films.*

Film thickness (nm)	Forward RF power (W)	Substrate bias voltage (V)	Target bias voltage (V)	Deposition time (s)
5	750	–200	–1500	30
10	750	–200	–1480	60
20	750	–200	–1400	120
35	750	–200	–1500	210

*working pressure = 3 mTorr, Ar gas flow rate = 20 sccm

Figure Captions

Fig. 1. AFM surface topography images of FCVA *a*-C films of thickness h equal to (a) 6–7 nm, (b) 10 nm, (c) 20 nm, and (d) 35 nm. (In-plane scale is in μm , whereas out-of-plane scale is in nm.)

Fig. 2. AFM surface topography images of RF sputtered *a*-C films of thickness h equal to (a) 5 nm, (b) 10 nm, (c) 20 nm, and (d) 35 nm. (In-plane scale is in μm , whereas out-of-plane scale is in nm.)

Fig. 3. Surface roughness versus thickness of FCVA and RF sputtered *a*-C films.

Fig. 4. Coefficient of friction versus sliding distance and load of FCVA and RF sputtered *a*-C films of thickness h equal to (a),(e) 5–7 nm, (b),(f) 10 nm, (c),(g) 20 nm, and (d),(h) 35 nm.

Fig. 5. Steady-state coefficient of friction versus load of FCVA and RF sputtered *a*-C films of thickness h equal to (a) 5–7 nm, (b) 10 nm, (c) 20 nm, and (d) 35 nm.

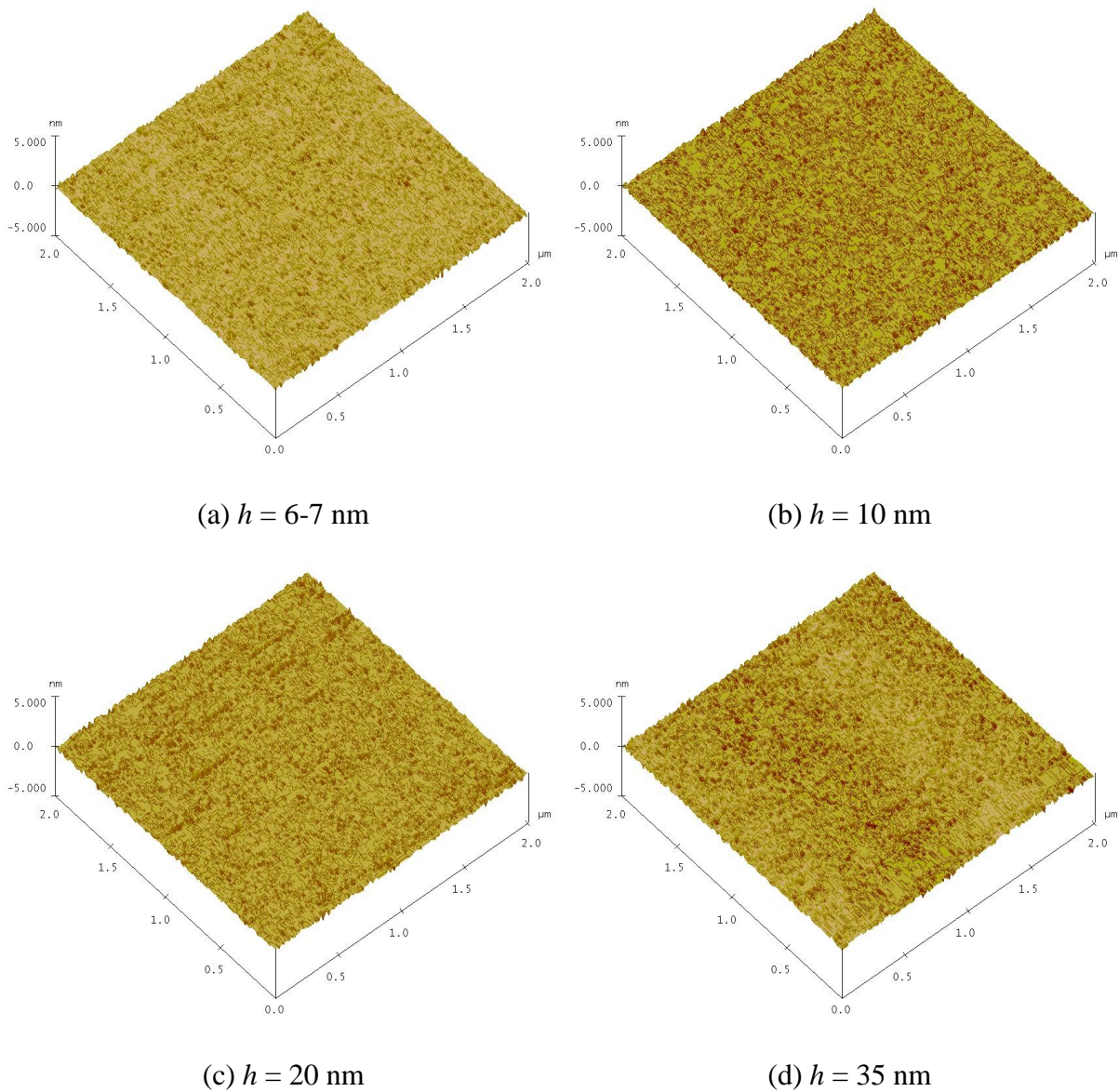


Fig. 1. AFM surface topography images of FCVA *a*-C films of thickness h equal to (a) 6–7 nm, (b) 10 nm, (c) 20 nm, and (d) 35 nm. (In-plane scale is in μm , whereas out-of-plane scale is in nm.)

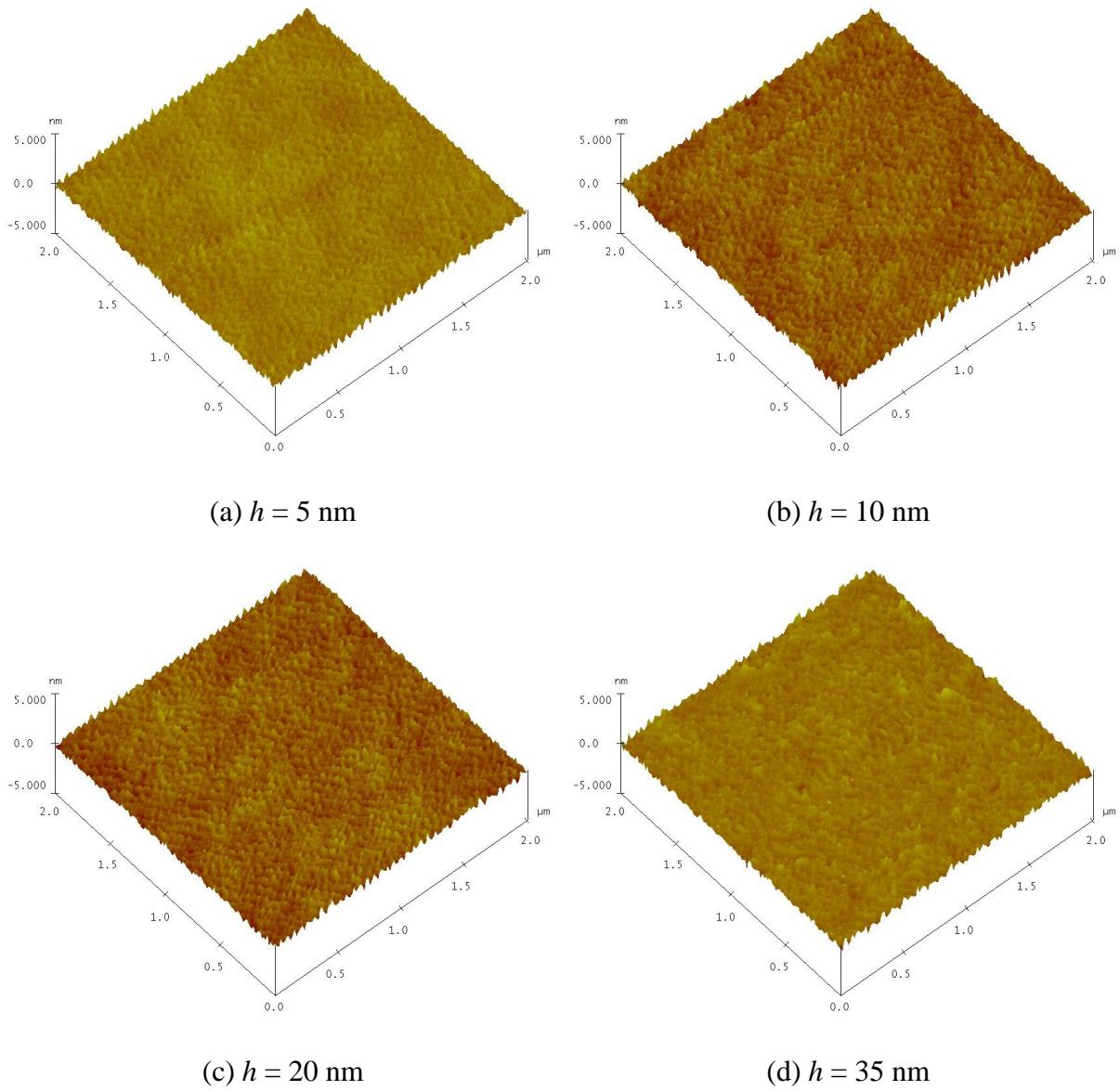


Fig. 2. AFM surface topography images of RF-sputtered *a*-C films of thickness h equal to (a) 5 nm, (b) 10 nm, (c) 20 nm, and (d) 35 nm. (In-plane scale is in μm , whereas out-of-plane scale is in nm.)

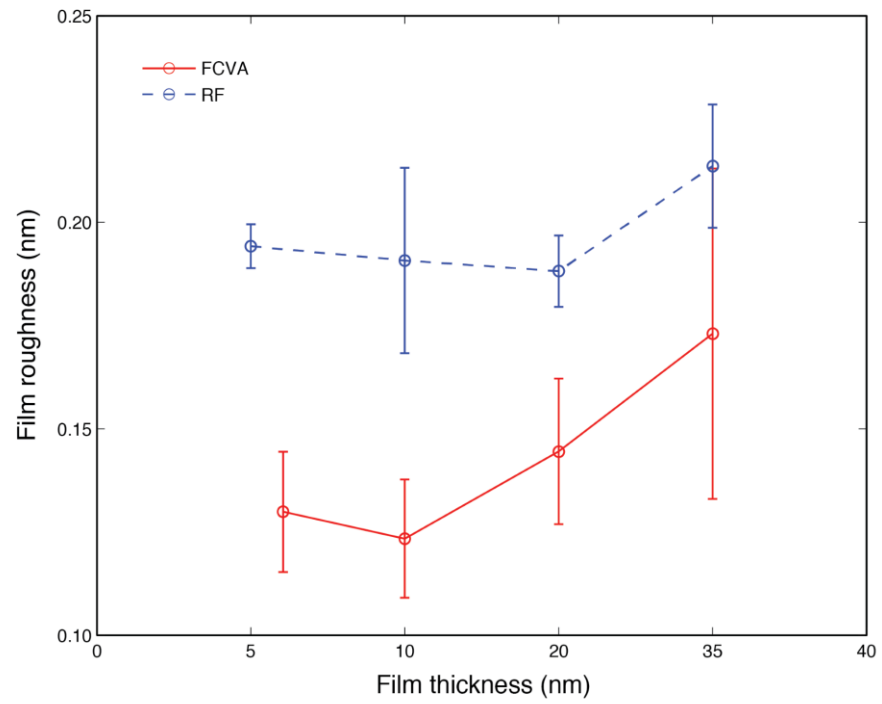


Fig. 3. Surface roughness versus thickness of FCVA and RF sputtered *a*-C films.

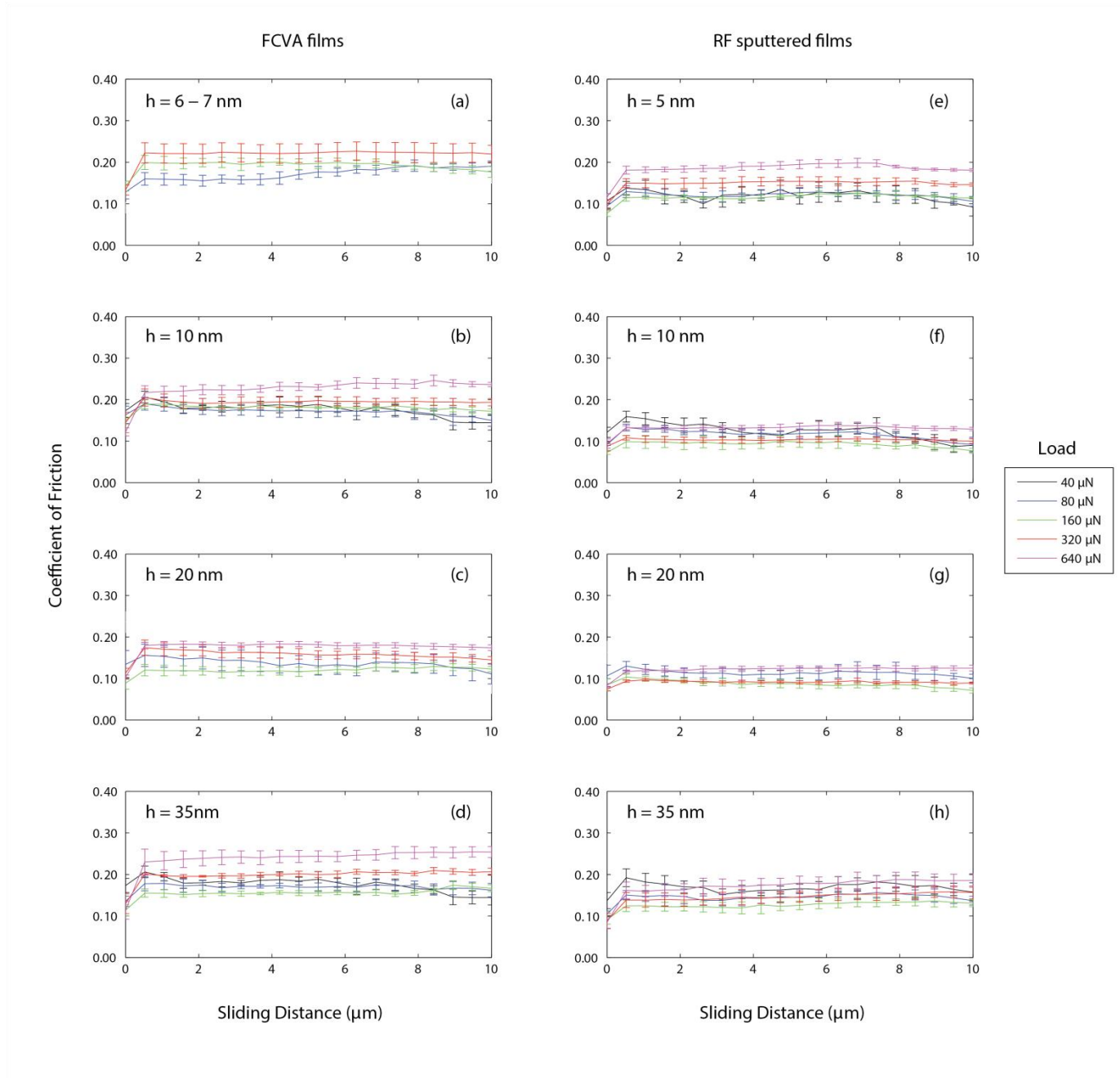


Fig. 4. Coefficient of friction versus scratch distance and load of FCVA and RF-sputtered a -C films of thickness h equal to (a),(e) 5–7 nm, (b),(f) 10 nm, (c),(g) 20 nm, and (d),(h) 35 nm.

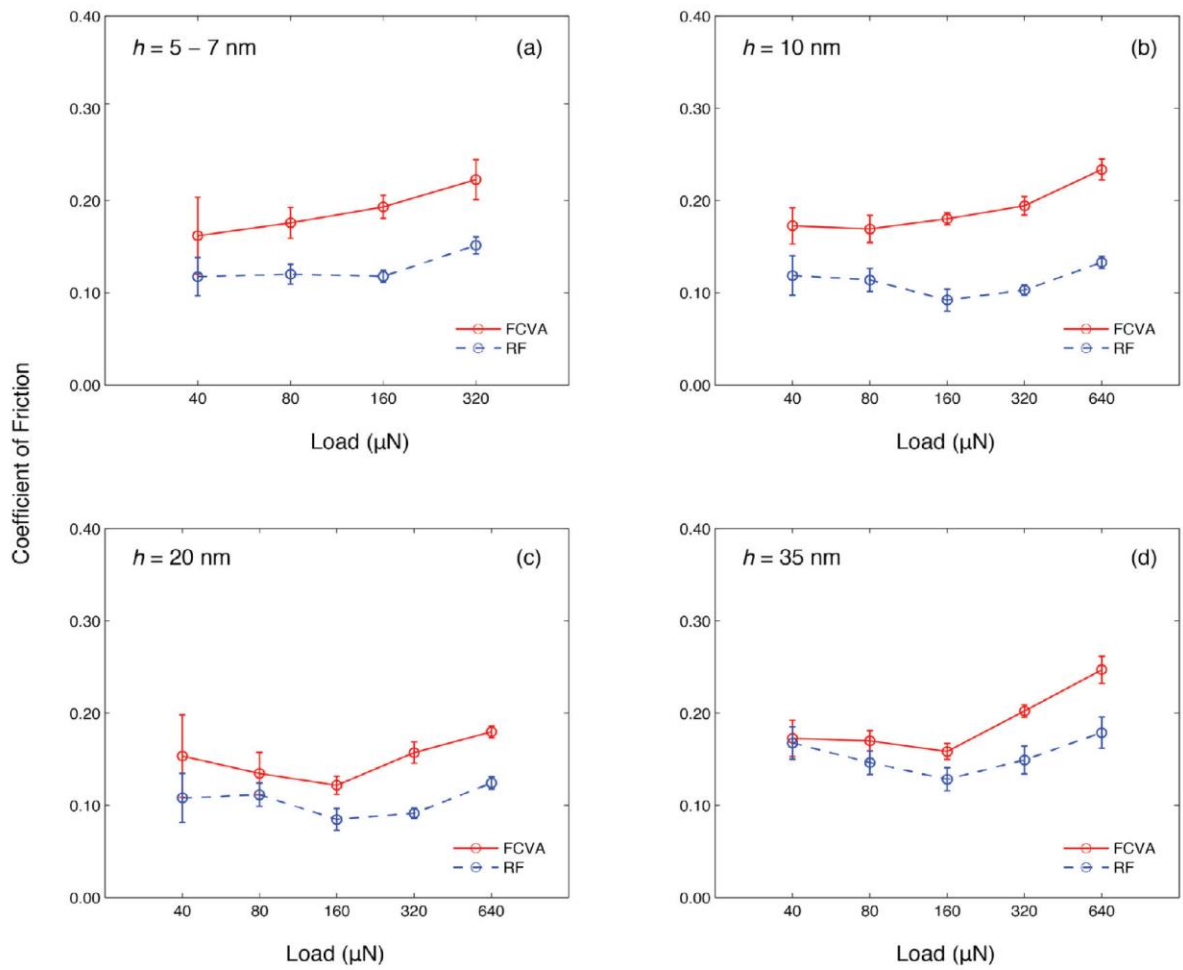


Fig. 5. Steady-state coefficient of friction versus load of FCVA and RF sputtered *a*-C films of thickness h equal to (a) 5–7 nm, (b) 10 nm, (c) 20 nm, and (d) 35 nm.